How Slice Stretching arises when Maximally Slicing the Schwarzschild Spacetime with Vanishing Shift

Bernd Reimann[1, 2]

[1]Max Planck Institut für Gravitationsphysik, Albert Einstein Institut, Am Mühlenberg 1, 14476 Golm, Germany
[2]Instituto de Ciencias Nucleares, Universidad Nacional Autónoma de México, A.P. 70-543, México D.F. 04510, México

(Dated: April 28, 2004)

When foliating the extended Schwarzschild spacetime with maximal slices while using zero shift, slice stretching effects such as slice sucking and slice wrapping arise. These effects are due to the differential infall of Eulerian observers and can be quantified for arbitrary spatial coordinates in the context of even boundary conditions. As examples logarithmic and isotropic grid coordinates are discussed. For boundary conditions where the lapse arises as a linear combination of odd and even lapse, two integrals are introduced which characterize the overall slice stretching. Favorable boundary conditions are then derived which make slice stretching occur late in numerical simulations. Allowing the lapse to become negative, this requirement leads to lapse functions which approach at late times the odd lapse corresponding to the static Schwarzschild metric. Demanding in addition that a numerically favorable lapse remains non-negative, as result the average of odd and even lapse is obtained. At late times the lapse with zero gradient at the puncture arising for the puncture evolution is precisely of this form. Finally a one-parameter family of boundary conditions is studied numerically and agreement with analytical results is found.

PACS numbers: 04.20.Cv, 04.25.Dm, 04.70.Bw, 95.30.Sf Preprint number: AEI-2004-035

I. INTRODUCTION

When a singularity avoiding lapse together with a vanishing shift is used to evolve a spacetime containing a physical singularity, the foliation is of pathological nature [1, 2, 3]. A first effect referred to as "slice sucking" consists of the "outward"-drifting of coordinate locations as the corresponding Eulerian observers are falling toward the singularity. This differential infall leads to large proper distances in between neighboring observers, creating large gradients in the radial metric function, the so-called "slice wrapping".

The overall effect is referred to as "slice stretching" and, being a geometric property of the slicing, is present independently of the existence of a numerical grid [4]. Its appearance has unpleasant consequences when numerically evolving say the Schwarzschild black hole spacetime: Due to slice sucking the coordinate location of e.g. the event horizon is found to move outward and the outer region continuously decreases in coordinate size. This not only is wasting numerical resources but might cause problems as outer boundary conditions assuming nearly flat space and implemented at a fixed coordinate location become inappropriate and fail. Furthermore, not being able to resolve with a finite number of grid points the developing steep gradients in components of the 3-metric, numerical inaccuracies caused by slice wrapping force a finite differencing code to crash.

Following up on earlier work done together with B. Brügmann, [5, 6, 7], in the present paper one particular singularity avoiding slicing is looked at, namely maximal slicing corresponding to the condition that the mean extrinsic curvature of the slices vanishes at all times [8]. This geometrically motivated choice of the lapse function has been used frequently in numerical relativity, for simulations of a single Schwarzschild black hole see e.g. [2, 3, 9, 10, 11, 12].

For Schwarzschild, and by including electric charge also for Reissner-Nordström, the maximal slices can be constructed analytically [9, 13, 14, 15]. For those spacetimes it is hence possible to examine slice stretching effects on an analytic level. The discussion throughout this paper is restricted to Schwarzschild, but since the same notation as in [5, 6, 7] is used, the results carry over in a straightforward way to Reissner-Nordström. Furthermore, only evolutions with vanishing shift are treated. Its generalization to non-trivial shifts - in order to study to what extent slice stretching effects can be avoided - will be the subject of a further paper [16].

In the following the maximal slices of the Schwarzschild spacetime are re-derived in the radial gauge and the transformation to an Eulerian line element characterized by a vanishing shift is given. Performing a late time analysis as in [6] based on [13], it is shown here that slice stretching arises at the throat of the Einstein-Rosen bridge [17].

Assuming symmetry with respect to the throat in order to fix its location in Eulerian coordinates by an isometry condition, it is then possible to quantify slice sucking and wrapping at the event horizon acting as a "marker". Examples of spatial coordinates to be discussed in the context of even boundary conditions are logarithmic grid coordinates (explaining numerical observations of e.g. [10, 12]) and isotropic grid coordinates (extending the study of [6]).

For boundary conditions other than the even ones, however, this analysis is more involved as one important example, the so-called puncture evolution, shows [6]. There black hole puncture data is evolved using a lapse with zero gradient at the "puncture", i.e. the compacti-

fied left-hand infinity. The corresponding lapse function is referred to as "zgp" or puncture lapse.

Focusing on boundary conditions where the lapse arises as superposition of odd and even lapse, two integrals characterizing the overall slice stretching are introduced. It is then shown that for "favorable" boundary conditions the slice stretching effects can occur arbitrarily late in numerical simulations. Here the lapse at late times has to approach the odd lapse, the latter corresponding to the static Schwarzschild metric and, being antisymmetric with respect to the throat, having negative values in the left-hand part of the spacetime. The numerical implementation of a lapse function which is partially negative, however, has been found to be unstable in at least two examples [18, 19]. Demanding hence in addition that a "numerically favorable" lapse should be non-negative, for latest possible occurrence of slice stretching a lapse being the average of odd and even lapse is obtained. One should note here that the puncture lapse is at late times characterized precisely by this condition.

Finally a one-parameter family of boundary conditions "ranging from odd to even" is studied numerically and the analytically predicted overall slice stretching is observed.

The paper is organized as follows: In Sec. II the maximal slices of the Schwarzschild spacetime are re-derived and the origin of slice stretching effects is pointed out. In Sec. III slice stretching effects are studied, concentrating in Subsec. III A on even boundary conditions and discussing logarithmic and isotropic grid coordinates explicitly. The overall slice stretching is quantified in Subsec. III B and boundary conditions are derived which make those effects occur late in numerical simulations. As examples the puncture lapse and a one-parameter family of boundary conditions are discussed. The results are summarized in Sec. IV.

II. MAXIMAL SLICES OF THE SCHWARZSCHILD SPACETIME

A. Radial gauge

Following [13] and starting from the Schwarzschild metric in Schwarzschild coordinates $\{t, r, \theta, \phi\}$,

$$ds^2 = -f(r)dt^2 + \frac{1}{f(r)}dr^2 + r^2 d\Omega^2 \quad \text{with} \quad f(r) = 1 - \frac{2M}{r}, \tag{1}$$

the maximal slices of this spacetime are most easily derived as level sets of the form

$$\sigma = t - t(\tau, r) = \text{const}. \tag{2}$$

Here the hypersurfaces are labeled by time at infinity τ and one has to examine the behavior of the normal

$$n = N\nabla\left(t - t(\tau, r)\right) = N\left(dt - \frac{\partial t}{\partial r}dr\right). \tag{3}$$

Making use of the line element (1), the normalization N is fixed by demanding

$$n_\mu n^\mu = N^2\left(-\frac{1}{f(r)} + f(r)\left(\frac{\partial t}{\partial r}\right)^2\right) = -1. \tag{4}$$

As pointed out in [13], N can also be considered the boost function of the static Killing vector $\frac{\partial}{\partial t}$ relative to $\sigma = \text{const}$,

$$N = -n_\mu\left(\frac{\partial}{\partial t}\right)^\mu. \tag{5}$$

Calculating the trace of the extrinsic curvature, K turns out to be given by

$$K = -\nabla_\mu n^\mu = \frac{1}{r^2}\frac{d\left[\frac{-r^2 f(r)\frac{\partial t}{\partial r}}{\sqrt{\frac{1}{f(r)} - f(r)\left(\frac{\partial t}{\partial r}\right)^2}}\right]}{dr}. \tag{6}$$

Demanding for maximal slicing $K \equiv 0$, the term in the brackets of (6) obviously has to be a function of time only to be denoted by $C(\tau)$. Hence

$$\frac{\partial t}{\partial r}(\tau, r) = -\frac{C(\tau)}{f(r)\sqrt{r^4 f(r) + C^2(\tau)}} \tag{7}$$

is found, which has to be integrated by imposing boundary conditions in order to obtain the level sets (2).

Furthermore, using the future normal of the foliation, $n_\mu = -\alpha\nabla_\mu\tau$, and writing the static Killing vector as $\left(\frac{\partial}{\partial t}\right)^\mu = Nn^\mu + \xi^\mu$ with $\xi_\mu n^\mu = 0$, the lapse can be obtained as

$$\alpha(\tau, r) = N(\tau, r)\frac{\partial t}{\partial \tau}. \tag{8}$$

Here N by the normalization (4) is given by

$$N(\tau, r) = \pm\sqrt{f(r) + \frac{C^2(\tau)}{r^4}} = \pm\frac{\sqrt{p_C(r)}}{r^2} \tag{9}$$

when introducing for convenience the polynomial

$$p_C(r) = r^4 f(r) + C^2 = r^4 - 2Mr^3 + C^2, \tag{10}$$

the subscript C denoting its dependence on C and hence on τ. Together with the radial metric component

$$\gamma(\tau, r) = \frac{r^4}{p_C(r)} \tag{11}$$

and the shift

$$\beta(\tau, r) = \frac{\alpha(\tau, r)\gamma(\tau, r)}{r^2}C(\tau) \tag{12}$$

the maximal slices in the radial gauge

$$ds^2 = \left(-\alpha^2 + \frac{\beta^2}{\gamma}\right)d\tau^2 + 2\beta\, d\tau dr + \gamma\, dr^2 + r^2\, d\Omega^2 \tag{13}$$

have been derived.

Furthermore, as pointed out in [20], the radial and angular components of the extrinsic curvature turn out to be given by

$$K^r_r = -2\frac{C}{r^3} \quad \text{and} \quad K^\theta_\theta = K^\phi_\phi = \frac{C}{r^3}, \tag{14}$$

respectively.

B. Eulerian observers

Next the spatial Schwarzschild coordinate r on the maximal slices shall be substituted by a spatial coordinate z corresponding to Eulerian observers. Applying a transformation of the form $r = r(\tau, z)$, the lapse $\alpha = \alpha(\tau, r(\tau, z))$ is still given by (8) and the line element is characterized by a vanishing shift,

$$ds^2 = -\alpha^2\, d\tau^2 + G\, dz^2 + r^2\, d\Omega^2. \tag{15}$$

In the context of maximal slicing, $K \equiv 0$, by contracting the evolution equation for the extrinsic curvature, one immediately obtains the statement that for zero shift the determinant of the 3-metric has to be time-independent. Hence the singularity avoiding property of maximal slicing comes to light as the variation of the local volume remains fixed [21]. For this reason one can make for the radial metric component the ansatz

$$G(\tau, z) = \frac{H(z)}{r^4(\tau, z)} \tag{16}$$

where the function $H(z)$ depending on z only is determined by the initial data.

The coordinate transformation relating r and z is found by comparison of the radial part of (13) and (15). For fixed slice label C one can infer the ordinary differential equation

$$\left.\frac{dr}{dz}\right|_{C=\text{const}} = \pm\frac{\sqrt{p_C(r)}}{r^4}\sqrt{H(z)} \tag{17}$$

which can be integrated using the throat as lower integration limit by

$$\int_{r_C}^{r} \frac{y^4\, dy}{\sqrt{p_C(y)}} = \pm\int_{z_C}^{z} \sqrt{H(y)}\, dy. \tag{18}$$

Here the "+" or "-" sign applies for the right- or left-hand side of the throat, respectively. Furthermore, r_C and z_C denote the location of the throat in terms of Schwarzschild and Eulerian spatial coordinates.

Note that r_C is found as root of the polynomial $p_C(r)$, which implies $C(\tau = 0) = 0$ when starting with the throat of the Einstein-Rosen bridge coinciding initially with the event horizon at $r_{EH} = 2M$. The throat r_C, describing the "innermost" two-sphere on a slice labeled by C, never reaches the singularity at $r = 0$ as $r_{C_{lim}} = 3M/2$ is found in the limit of late times with C approaching

$$C_{lim} = \frac{3}{4}\sqrt{3}M^2 \tag{19}$$

as pointed out in [9]. Hence for the Schwarzschild spacetime the singularity avoidance of maximal slices becomes apparent, c.f. corollary 3.3 of [22].

The coordinate location of the throat in Eulerian coordinates depends in general also on C and is hence a function of time determined by boundary conditions. Here the behavior of z_C can be found by demanding the transformation (18) to be consistent with the requirement of a vanishing shift as discussed in more detail in [6].

By making use of (16), however, it is possible to describe in the late time limit the profile of the radial metric component near the throat since the latter approaches the value $r_{C_{lim}} = 3M/2$ there.

Furthermore, according to (14) for fixed time at infinity the peak in the profiles of the extrinsic curvature components arises at the throat. For $K^\theta_\theta = -K^r_r/2$ in the limit $C \to C_{lim}$ its value there is obtained as $C_{lim}/r^3_{C_{lim}} = 2\sqrt{3}/9M \approx 0.3849/M$.

C. Origin and indicators of slice stretching

As stated in [13], when demanding antisymmetry with respect to the throat maximal slices are found where C being purely gauge can be chosen independently of time at infinity. Here the 3-metric is given time-independently by the initial data and the odd lapse can be written as

$$\alpha_{odd} = \pm\frac{\sqrt{p_C(r)}}{r^2}. \tag{20}$$

In particular, the odd lapse vanishes at the throat and is positive/negative in the original/extended part of the Schwarzschild spacetime to yield the values plus/minus one at right-/left-hand spatial infinity.

Excluding odd boundary conditions where no slice stretching occurs, for a discussion of the late time behavior of maximal slicing instead of the slice label C it turns out to be convenient to introduce δ as in [13] by

$$\delta = r_C - r_{C_{lim}}. \tag{21}$$

The late time limit $\tau \to \infty$ then can be said to correspond to the limit $\delta \to 0$ as the maximal slices approach the limiting slice $r = r_{C_{lim}} = 3M/2$ asymptotically.

By analyzing in this limit the transformation (18) and the behavior of the 3-metric (15), slice stretching effects can be studied. As in [6] this discussion will for simplicity be restricted to the throat and the event horizon acting as markers for slice sucking and wrapping.

In this reference it has been shown that integrating up to the event horizon, in the limit $\delta \to 0$ the integral on the left-hand side of (18) diverges like

$$\int_{r_C}^{r_{EH}} \frac{y^4\, dy}{\sqrt{p_C(y)}} = -C_{lim}\Omega \ln\left[\frac{\delta}{M}\right] + \mathcal{O}(1) \qquad (22)$$

where Ω is a further fundamental constant given by

$$\Omega = \frac{3}{4}\sqrt{6}M. \qquad (23)$$

The proof of this statement is rather lengthy, see [6] for details. The divergence proportional to $\ln[\delta]$ can be understood, however, by observing that for $C \to C_{lim}$ the lower limit of integration r_C becomes a double counting root of the polynomial $p_C(r)$, the root of which appears in the denominator of the integrand of (22). Since the upper limit of integration essentially plays no role in this expansion, one should note that any isosurface described by a constant value of $r = \text{const} \geq r_{EH}$ could be used in the following as a marker for slice stretching effects.

The diverging term picked up at the throat in (22) is the origin of slice stretching. Those effects are hence a feature of the region near the throat. Denoting the location of the right- and left-hand event horizon by $z^{\pm}_{CEH}$, the subscript C referring again to its time dependence, from the coordinate transformation (18) in the context of (22) one can infer

$$\pm \int_{z_C}^{z^{\pm}_{CEH}} \sqrt{H(y)}\, dy = -C_{lim}\Omega \ln\left[\frac{\delta}{M}\right] + \mathcal{O}(1). \qquad (24)$$

Hence slice sucking is present as in the limit $\delta \to 0$ the event horizon is driven away from the throat by a term diverging logarithmically with δ.

With throat and event horizon moving away from each other, in general also slice wrapping effects in between z_C and $z^{\pm}_{CEH}$ show up in the form of an unbounded growth and/or a rapidly steepening gradient in the radial metric component. To study those, note that in numerical implementations often a time-independent conformal factor $\Psi^4(z)$ is factored out from the 3-metric to focus on the dynamical features of the metric rather than the static singularity. In order to discuss the behavior of the rescaled 3-metric, it is convenient to introduce

$$g(\tau, z) = \frac{G(\tau, z)}{\Psi^4(z)} \quad \text{and} \quad h(z) = \frac{H(z)}{\Psi^4(z)} \qquad (25)$$

which according to (16) are related by

$$g(\tau, z) = \frac{h(z)}{r^4(\tau, z)}. \qquad (26)$$

Differentiating now (26) with respect to z by making use of the product rule and (17), one can extend the study of [6] by analyzing in addition to the value also the gradient of g. In particular, at the throat one obtains

$$\left.\frac{dg}{dz}\right|_{z_C} = \frac{1}{r_C^4} \left.\frac{dh}{dz}\right|_{z_C} \qquad (27)$$

since dr/dz vanishes there. Furthermore, at the right- and left-hand event horizon the gradient

$$\left.\frac{dg}{dz}\right|_{z^{\pm}_{CEH}} = \frac{1}{r_{EH}^4} \left.\frac{dh}{dz}\right|_{z^{\pm}_{CEH}} \mp \frac{4Ch(z^{\pm}_{CEH})\sqrt{H(z^{\pm}_{CEH})}}{r_{EH}^9} \qquad (28)$$

is found.

Although not obvious from the expressions (26), (27) and (28), one in general can expect both g and dg/dz to diverge in the limit of late times at the throat and/or the event horizon. This happens as the functions H, h and dh/dz evaluated there usually grow without bounds while the Schwarzschild radius at the throat is approaching $r_{C_{lim}} = 3M/2$ and at the event horizon is given by $r_{EH} = 2M$. In Sec. III slice wrapping will be worked out explicitly for two coordinate choices used frequently in numerical relativity.

In order to describe as a function of time at infinity the slice stretching arising from (22) and showing up e.g. in (24), it is in addition necessary to specify the relationship $\delta(\tau)$ by imposing boundary conditions. Slice stretching for even boundary conditions will be discussed in Subsec. III A and favorable boundary conditions, where the effects described in terms of δ show up late in terms of τ, will be derived in Subsec. III B.

III. SLICE STRETCHING EFFECTS

A. EVEN BOUNDARY CONDITIONS

Height function

Treating the extended and the original part of the Schwarzschild spacetime on equal footing by demanding symmetry with respect to the throat, even boundary conditions are found naturally. Here in a Carter-Penrose diagram the throat has to remain on the symmetry axis characterized by $t = 0$, see Fig. 4 in [5]. As in [9, 13] by integrating (7) for the even "height function" one obtains the integral

$$t_{even}(C, r) = -\int_{r_C}^{r} \frac{C\, dy}{f(y)\sqrt{p_C(y)}} \qquad (29)$$

defined for $r \geq r_C$. Note that the integration across the pole at r_{EH} is taken in the sense of the principal value and the corresponding slices extend smoothly through both the event horizon r_{EH} and the throat r_C. Since proper time is measured at spatial infinity, from (29) in

the limit $r \to \infty$ one can infer the relationship

$$\tau_{even}(C) = -\int_{r_C}^{\infty} \frac{C\, dy}{f(y)\sqrt{p_C(y)}} \tag{30}$$

between τ_{even} and C.

Late time analysis

As shown in [13] by expanding τ_{even} in terms of δ in the late time limit $C \to C_{lim}$, i.e. for $\delta \to 0$, time at infinity is diverging like

$$\tau_{even}(\delta) = -\Omega \ln\left[\frac{\delta}{M}\right] + \Lambda + \mathcal{O}(\delta) \tag{31}$$

where Ω has been defined already in (23) and Λ is a constant with the analytic value given by

$$\frac{\Lambda}{M} = \frac{3}{4}\sqrt{6}\ln\left[18(3\sqrt{2}-4)\right] - 2\ln\left[\frac{3\sqrt{3}-5}{9\sqrt{6}-22}\right]. \tag{32}$$

Here the divergence of τ_{even} proportional to $\ln[\delta]$ arises at the throat for the same reason as pointed out for the expansion (22).

As later on expansions in δ will be studied, one should observe that solving in (31) for δ, in leading order with

$$\frac{\delta}{M} = \exp\left[\frac{\Lambda}{\Omega}\right]\exp\left[-\frac{\tau_{even}}{\Omega}\right] + \mathcal{O}(\exp\left[-2\frac{\tau_{even}}{\Omega}\right]) \tag{33}$$

an exponential decay of δ with τ_{even} on the fundamental timescale Ω is found.

Lapse function

The even lapse arises from (8) and is given by

$$\alpha_{even} = \pm\frac{\sqrt{p_C(r)}}{r^2}\frac{\partial t_{even}}{\partial C}\frac{dC}{d\tau_{even}}. \tag{34}$$

Studying its late time behavior as in [13] and [6], it turns out that α_{even} collapses at the throat in order $\mathcal{O}(\delta)$ and hence in leading order decays exponentially in time on the fundamental timescale Ω there to avoid the singularity. By symmetry, at both left- and right-hand event horizon in the limit of late times the finite value $C_{lim}/r_{EH}^2 = 3\sqrt{3}/16 \approx 0.3248$ is found, and by construction the even lapse approaches unity at both infinities. For a particular choice of spatial coordinates, namely isotropic grid coordinates, the time evolution of the even lapse is shown in Fig. 1.

Slice stretching in the limit of late times

The discussion of slice stretching is particularly simple for even boundary conditions as due to an isometry condition the location of the throat in Eulerian coordinates is given time-independently by its initial value $z_{\forall C} = z_{EH} = \text{const}$. From the expansion (24) in the context of (33) one can then infer

$$\pm\int_{z_{EH}}^{z^{\pm}_{CEH}} \sqrt{H(y)}\, dy = C_{lim}\tau_{even} + \mathcal{O}(1). \tag{35}$$

Hence in the limit of late times slice sucking is present since the event horizon is driven away from z_{EH} by a term diverging proportional to τ_{even}.

From (26) one can then see that very little evolution is present at the throat since g only grows to $(4/3)^4 \approx 3.1605$ times its initial value there as the Schwarzschild radius declines from $r_{EH} = 2M$ to $r_{C_{lim}} = 3M/2$. Furthermore, by a symmetry argument the gradient of g at the throat vanishes.

In order to study slice wrapping at the event horizon, it is then best to look at specific spatial coordinates such as logarithmic or isotropic grid coordinates which both are used frequently in numerical simulations.

First example: Logarithmic grid coordinates

Logarithmic grid coordinates η [23] arise when implementing initially the Schwarzschild geometry in terms of logarithmic coordinates corresponding to the 3-metric

$${}^{(3)}ds^2 = \Psi^4(\eta)(d\eta^2 + d\Omega^2). \tag{36}$$

Here at $\tau_{even} = 0$ with the conformal factor given by

$$\Psi(\eta) = \sqrt{2}\cosh\left[\frac{\eta}{2}\right]\sqrt{M} \tag{37}$$

the relationship

$$r(\tau_{even} = 0, \eta) = \Psi^2(\eta) \tag{38}$$

between η and the Schwarzschild radius r is found. Independently of time, the throat is located at $\eta_{\forall C} = \eta_{EH} = 0$ and the isometry

$$\eta \longleftrightarrow -\eta \tag{39}$$

is mapping the right-hand part of the spacetime to the left-hand part and vice versa.

With $G = \Psi^{12}/r^4$ one may readily verify

$$H(\eta) = \Psi^{12}(\eta) \quad \text{and} \quad h(\eta) = \Psi^8(\eta) \tag{40}$$

and observe that the rescaled radial component of the metric grows from unity to the finite value $(4/3)^4 \approx 3.1605$ at the origin being the location of the

throat, where in the limit of late times g behaves like $\Psi^8/r^4_{C_{lim}}$. Furthermore, since $g = \Psi^8/r^4$ is even, obviously its derivative vanishes there.

Discussing slice sucking at the event horizon, from (35) and (40) it turns out that in leading order the event horizon moves outward like

$$\eta^{\pm}_{CEH} \simeq \pm\frac{1}{3}\ln\left[\frac{24C_{lim}\tau_{even}}{M^3}\right] = \mathcal{O}\left(\ln\left[\tau^{1/3}_{even}\right]\right). \quad (41)$$

Inserting this result in (26) while using (40), slice wrapping is taking place there as g in leading order grows according to

$$g|_{\eta^{\pm}_{CEH}} = \frac{\Psi^8(\eta^{\pm}_{CEH})}{r^4_{EH}} = \mathcal{O}\left(\tau^{4/3}_{even}\right). \quad (42)$$

Furthermore, making use of (28) and again (40), it turns out that a rapidly steepening gradient at the event horizon is present as

$$\left.\frac{dg}{d\eta}\right|_{\eta^{\pm}_{CEH}} \simeq \mp\frac{4C_{lim}\Psi^{14}(\eta)}{r^9_{EH}} = \mathcal{O}\left(\tau^{7/3}_{even}\right) \quad (43)$$

is found.

These analytical statements should be compared with numerical results as e.g. in [10, 12]. Note that in these simulations it is rather slice wrapping than slice sucking which causes the runs to crash quite early. This can now be understood by the argument that the event horizon is moving outward only moderately whereas a rapidly steepening gradient in g is found there together with a peak growing slightly further inside.

Second example: Isotropic grid coordinates

Isotropic grid coordinates x [23] have been constructed in [5] such that the 4-metric coincides at all times with output from a numerical evolution of black hole puncture data. Here initially the 3-metric

$${}^{(3)}ds^2 = \Psi^4(x)(dx^2 + x^2\, d\Omega^2) \quad (44)$$

is implemented making use of isotropic coordinates. So with the conformal factor

$$\Psi(x) = 1 + \frac{M}{2x} \quad (45)$$

it turns out that x at $\tau_{even} = 0$ is related to the Schwarzschild radius by

$$r(\tau_{even} = 0, x) = x\Psi^2(x). \quad (46)$$

Since for even boundary conditions also during the evolution isotropic and logarithmic grid coordinates are related by

$$x = \frac{M}{2}\mathrm{e}^{\eta}, \quad (47)$$

one can see that the region $\eta \leq 0$ is compactified to $0 \leq x \leq M/2$ and $\eta \geq 0$ is mapped to $x \geq M/2$. Here due to the isometry

$$x \longleftrightarrow \frac{M^2}{4x} \quad (48)$$

the throat is fixed for all times at $x_{\forall C} = x_{EH} = M/2$ and the puncture at $x = 0$ is simply a compactified image of spatial infinity.

From $G = x^4\Psi^{12}/r^4$ then follows

$$H(x) = x^4\Psi^{12}(x) \quad \text{and} \quad h(x) = x^4\Psi^8(x) \quad (49)$$

and as for logarithmic grid coordinates one can observe that $g = x^4\Psi^8/r^4$ at the throat grows from unity to $(4/3)^4 \approx 3.1605$ while due to the isometry a vanishing gradient is present there.

When analyzing slice stretching at the event horizon, it turns out that for the outward-movement of the right-hand event horizon in leading order by using (35) and (49) (or alternatively (41) and (47)) for its location

$$x^{+}_{CEH} \simeq (3C_{lim}\tau_{even})^{1/3} = \mathcal{O}\left(\tau^{1/3}_{even}\right) \quad (50)$$

is obtained. The left-hand event horizon, however, due to the isometry (48) approaches the puncture like

$$x^{-}_{CEH} = \frac{M^2}{4x^{+}_{CEH}} = \mathcal{O}\left(\tau^{-1/3}_{even}\right). \quad (51)$$

For both right- and left-hand event horizon the rescaled radial metric component g coincides and in leading order diverges according to

$$g|_{x^{\pm}_{CEH}} = \frac{x^{\pm\,4}_{CEH}\Psi^8(x^{\pm}_{CEH})}{r^4_{EH}} = \mathcal{O}\left(\tau^{4/3}_{even}\right). \quad (52)$$

Analyzing now the gradient of g at the event horizon, the particular problem of isotropic grid coordinates in the context of even boundary conditions comes to light. Whereas according to (28) at the right-hand event horizon the gradient

$$\left.\frac{dg}{dx}\right|_{x^{+}_{CEH}} \simeq -\frac{4C_{lim}x^{+\,6}_{CEH}}{r^9_{EH}} = \mathcal{O}\left(\tau^2_{even}\right) \quad (53)$$

is found, at the left-hand event horizon the derivative

$$\begin{aligned}\left.\frac{dg}{dx}\right|_{x^{-}_{CEH}} &= \frac{dx^{+}_{CEH}}{dx^{-}_{CEH}}\left.\frac{dg}{dx}\right|_{x^{+}_{CEH}} \\ &= -\frac{M^2}{4x^{-\,2}_{CEH}}\left.\frac{dg}{dx}\right|_{x^{+}_{CEH}} = \mathcal{O}\left(\tau^{8/3}_{even}\right)\end{aligned} \quad (54)$$

is diverging even more rapidly.

As can be seen in Fig. 1, a numerically very cumbersome "double peak" in the profile of g is developing which due to slice wrapping in the compactified left-hand part

of the Schwarzschild spacetime prevents long-lasting simulations. In Subsec. III B an analysis of other boundary conditions will show, however, that initially selecting isotropic coordinates can nevertheless be a "good" coordinate choice, since the numerically unfavorable behavior described so far can be blamed mainly on the use of even boundary conditions. Applying for the puncture evolution more adapted "zgp" boundary conditions, i.e. demanding symmetry at the puncture and obtaining a vanishing gradient of the lapse there, results in significantly better slice stretching behavior as can be seen in Fig. 2.

With the Schwarzschild radius at the throat approaching the value $r_{C_{lim}} = 3M/2$ in the limit of late times, by making use of $g = x^4\Psi^8/r^4$ it is (independently of the boundary conditions) possible to describe the limiting profile of g near the throat by $x^4\Psi^8/r^4_{C_{lim}}$. The latter has been plotted in both Fig. 1 and 2 as dotted line.

In addition, extending the study of [6], the profiles of the radial and the angular component of the extrinsic curvature shall be discussed here (again for arbitrary boundary conditions). According to (14), for fixed time at infinity with $r \propto \frac{1}{x}$ for $\{r \to \infty, x \to 0\}$ both K^r_r and K^θ_θ near the puncture are of order $\mathcal{O}(x^3)$, whereas with $r = x$ for $\{r \to \infty, x \to \infty\}$ for large values of x they decay in order $\mathcal{O}(x^{-3})$. Furthermore, the peak in the profiles of the extrinsic curvature components is found at the throat. In the late time limit for $K^\theta_\theta = -K^r_r/2$ its value there is obtained as $C_{lim}/r^3_{C_{lim}} = 2\sqrt{3}/9M \approx 0.3849/M$, the latter being in excellent agreement with numerical results as shown in both Fig. 1 and 2.

B. FAVORABLE BOUNDARY CONDITIONS

Lapse constructed as a superposition of odd and even lapse

With the trace of the extrinsic curvature vanishing, $K \equiv 0$, the lapse arises for maximal slicing from the elliptic equation

$$\triangle\alpha = \nabla^i\nabla_i\alpha = R\alpha \tag{55}$$

where R is the 3-dimensional Ricci scalar. For fixed time at infinity, this condition is a second order linear ordinary differential equation. Hence, demanding the lapse to be one at spatial infinity in order to measure proper time there, when supplementing an additional boundary condition the lapse is completely determined.

With odd and even lapse two linearly independent lapse functions satisfying (55) have been found as pointed out in [13]. By the superposition principle it is then possible to construct a new lapse, normalized again to unity at right-hand infinity, by a linear combination

$$\alpha(\tau, r) = \Phi(\tau) \cdot \alpha_{even}(\tau, r) + (1 - \Phi(\tau)) \cdot \alpha_{odd}(\tau, r) \tag{56}$$

with a time-dependent "multiplicator function" $\Phi(\tau)$. An important example for such a superposition is the puncture lapse constructed in [5].

Height function

As shown in Subsec. II A, the maximal slicing condition fixes the partial derivative of t with respect to r as in (7) only, whereas boundary conditions have to be specified to obtain $t(\tau, r)$ by integration. The latter can always be written as the sum of the even height function and a "time translation function" $t_C(\tau)$ depending on time only,

$$t(\tau, r) = t_{even}(\tau, r) + t_C(\tau), \tag{57}$$

where time at infinity is measured again in the limit $r \to \infty$. As for $\tau = 0$ one starts with the time-symmetric $t = 0$ hypersurface, the function t_C vanishes initially and is determined during the evolution by boundary conditions. Furthermore, since the even height function vanishes at the throat during the evolution, t_C also represents the value of t at the throat. Hence the time translation function describes where the throat is found in a Carter-Penrose diagram, see for "zgp" boundary conditions Fig. 4 in [5].

Slice stretching integrals

Imposing boundary conditions, the multiplicator function $\Phi(\tau)$ in (56), the time translation function $t_C(\tau)$ in (57) and the location of the throat in terms of Eulerian coordinates are determined. Deriving z_C as a function of τ explicitly, however, is rather involved as one has to examine each boundary condition separately when analyzing the coordinate transformation (18) while making sure that the shift vanishes [6]. For a study of slice stretching at e.g. the event horizon, though, the location of the throat has to be determined first, since, as shown in Subsec. II C, the diverging term in the integral (24) being proportional to $\ln[\delta]$ and causing slice stretching is picked up at the throat.

Integrating metric quantities from the left-hand to the right-hand event horizon yields an alternative approach for a discussion of slice stretching while avoiding in an elegant way inconveniences involved in determining z_C as a function of time. Although such integrals can not provide items of information like the location of throat or event horizon and value or gradient of the radial metric component there, they are nevertheless excellent indicators for the overall slice stretching.

Here two such integrals shall be introduced, namely

$$\begin{aligned}
\mathcal{S}_H(\delta) &= \int_{z^-_{CEH}}^{z^+_{CEH}} \sqrt{H(y)}\, dy \\
&= 2\int_{r_C}^{r_{EH}} \frac{y^4\, dy}{\sqrt{p_C(y)}} \\
&= -2C_{lim}\Omega \ln\left[\frac{\delta}{M}\right] + \mathcal{O}(1)
\end{aligned} \tag{58}$$

and

$$\begin{aligned}\mathcal{S}_G(\delta) &= \int_{z^-_{CEH}}^{z^+_{CEH}} \sqrt{G(\tau,y)}\, dy \\ &= 2\int_{r_C}^{r_{EH}} \frac{y^2\, dy}{\sqrt{p_C(y)}} \\ &= -2\frac{C_{lim}\Omega}{r^2_{C_{lim}}} \ln\left[\frac{\delta}{M}\right] + \mathcal{O}(1). \end{aligned} \tag{59}$$

Whereas the first integral arises directly from the coordinate transformation (18) and essentially has been studied in (22) and (24) already, the second integral is in a more straightforward way related to slice sucking (since the left- and right-hand event horizon appear as limits of integration) and slice wrapping (since the integrand is the root of the radial metric component). So whereas for some analytical purposes making use of $\mathcal{S}_H$ might be preferable, for numerical studies of slice stretching $\mathcal{S}_G$ should be of particular interest. In order to locate both left- and right-hand event horizon on the maximal slices to calculate either (58) or (59) numerically, one can compute the Schwarzschild radius r from the prefactor of the angular part of the metric as e.g. in [5, 18] and identify an event horizon as isosurface with $r = r_{EH} = 2M$. Alternatively, since for the Schwarzschild spacetime event and apparent horizon coincide, for this task both apparent and event horizon finders can be used in principle.

Boundary conditions for late observation of slice stretching

The idea now is to obtain relationships between δ and τ which make the overall slice stretching, in terms of δ arising from (22) and expressed by integrals such as (58) or (59), occur late in terms of τ in numerical simulations. By specifying $\delta(\tau)$, however, boundary conditions for the lapse arise since the multiplicator function appearing in the linear combination (56) can be written as

$$\Phi(\delta) = \frac{\left(\frac{\partial t}{\partial \delta} - \frac{d\tau}{d\delta}\right)\frac{d\tau_{even}}{d\delta}}{\left(\frac{\partial t_{even}}{\partial \delta} - \frac{d\tau_{even}}{d\delta}\right)\frac{d\tau}{d\delta}} = \frac{\frac{d\tau_{even}}{d\delta}}{\frac{d\tau}{d\delta}}. \tag{60}$$

This expression one can readily verify making use of (8), (56) and (57). Assuming that a given numerical code for a chosen resolution can only handle a certain amount of overall slice stretching, the hope then is that longer lasting evolutions covering a greater portion of the spacetime can be obtained by imposing more favorable boundary conditions instead of even ones.

As one can see from (60), demanding that slice stretching effects show up later than for even boundary conditions with $-d\tau/d\delta > -d\tau_{even}/d\delta > 0$ implies that the multiplicator function has to be less than one, $0 \leq \Phi < 1$. Note that slice stretching can occur arbitrarily late with Φ approaching zero and the lapse arising in (56) being then essentially given by the odd lapse. Furthermore, if Φ for odd boundary conditions vanishes throughout the evolution, no slice stretching at all is found.

In particular, when looking at $\tau = \tau_{even} + t_C$, by making use of (31) one can readily verify that if the time translation function t_C is of order $\mathcal{O}(1)$, as for the even lapse an exponential decay of δ with τ is found. The overall slice stretching then can be expected to be similar to the one arising for even boundary conditions.

Adding, however, a term which diverges logarithmically with δ, i.e. $t_C \simeq -\tilde{\Omega}\ln[\delta/M]$, the exponential decay of δ takes place on a time scale given by the sum of Ω and $\tilde{\Omega}$. The corresponding multiplicator function for this choice of t_C is given by $\Phi \simeq \Omega/(\Omega+\tilde{\Omega})$. In principle with $\tilde{\Omega} \to \infty$ the new time scale can be made arbitrarily large to make slice stretching effects occur arbitrarily late. In this limit, however, one finds that with $\Phi \to 0$ the odd lapse is approached.

It is also possible to obtain in leading order not an exponential but a power-law decay of δ with τ, allowing for very moderate slice stretching behavior. Assuming that $t_C \simeq \delta^{-k}$, $k > 0$, then $\tau \simeq \delta^{-k}$ and $\Phi \simeq \Omega\delta^k/k$ are found. But note that for late times with $\delta \to 0$ again the odd lapse is approached.

Whereas it is possible to find boundary conditions such that the overall slice stretching occurs arbitrarily late, the corresponding lapse approaching the odd lapse might from the numerical point of view be disadvantageous as negative values of the lapse occur. For this reason a numerically favorable lapse in addition should be non-negative. Using (56) and the formulas (20) and (34) for odd and even lapse, one can show that demanding $\alpha \geq 0$ corresponds to $\Phi \geq 1/2$. Hence the power-law decay of δ is ruled out, but choosing $0 \leq \tilde{\Omega} \leq \Omega$ it is possible to find a lapse such that the time scale for the exponential decay of δ is up to twice the one obtained for even boundary conditions. In particular, the non-negative lapse showing latest possible occurrence of slice stretching is at late times given by the average of odd and even lapse.

First example: The puncture lapse

It is at this point essential to note that the puncture lapse discussed in [5] is precisely of this form and the puncture evolution of a Schwarzschild black hole is hence taking place in a numerically favorable manner. As shown in this reference, the multiplicator function of the "zgp" lapse is given by

$$\Phi = \frac{1}{2}\,\frac{\int_{r_C}^{\infty} \frac{y(y-3M)\,dy}{(y-\frac{3M}{2})^2\sqrt{p_C(y)}}}{\int_{r_C}^{\infty} \frac{y(y-3M)\,dy}{(y-\frac{3M}{2})^2\sqrt{p_C(y)}} + \frac{1}{M}}. \tag{61}$$

Here the integral appearing in both the numerator and denominator of (61) is diverging proportional to $1/\delta^2$ as

the throat in the limit of late times becomes a threefold root of the denominator of the integrand. For this reason the "zgp" multiplicator function is of the form $\Phi_{zgp} = 1/2 + \mathcal{O}(\delta^2)$ and the puncture lapse, being positive everywhere, arises at late times as average of odd and even lapse. Performing a late time analysis, it turns out that α_{zgp} collapses to zero in order $\mathcal{O}(\delta^2)$ at the puncture and the left-hand event horizon and in order $\mathcal{O}(\delta)$ at the throat. At the right-hand event horizon, as for even boundary conditions, the finite value $C_{lim}/r_{EH}^2 = 3\sqrt{3}/16 \approx 0.3248$ is found in the limit of late times, and the lapse approaches unity at spatial infinity, see [6] for details. The profile of the puncture lapse for the puncture evolution is shown in Fig. 2.

In [5] the "zgp" height function is derived as

$$t^{\pm}_{zgp}(C,r) = t_{even}(C,r) \pm (\tau_{even}(C) - \frac{C}{M}) \tag{62}$$

where time is measured at right-hand spatial infinity by

$$\tau_{zgp}(C) = 2\tau_{even}(C) - \frac{C}{M}. \tag{63}$$

Making use of the expansion (31) and $C = C_{lim} + \mathcal{O}(\delta^2)$, in leading order the exponential decay of δ with τ_{zgp} is with

$$\frac{\delta}{M} = \exp\left[\frac{2\Lambda M - C_{lim}}{2\Omega M}\right] \exp\left[-\frac{\tau_{zgp}}{2\Omega}\right] + \mathcal{O}(\exp\left[-\frac{\tau_{zgp}}{\Omega}\right]) \tag{64}$$

taking place on twice the fundamental timescale Ω.

For the puncture evolution the slice stretching behavior has been discussed in [6] from left to right at the left-hand event horizon, the throat and the right-hand event horizon. As shown there, in the limit $\tau_{zgp} \to \infty$ the left-hand event horizon is found at a finite value in between its initial location $x_{EH} = M/2$ and the puncture, whereas both throat and right-hand event horizon are moving outward like

$$x_C \simeq \left(\frac{3}{2} C_{lim} \tau_{zgp}\right)^{1/3} = \mathcal{O}\left(\tau_{zgp}^{1/3}\right) \tag{65}$$

and

$$x^+_{CEH} \simeq (3 C_{lim} \tau_{zgp})^{1/3} = \mathcal{O}\left(\tau_{zgp}^{1/3}\right), \tag{66}$$

respectively.

As x^-_{CEH} freezes at late times, also the rescaled radial metric component approaches a finite value there. At x_C and x^+_{CEH}, however, with $g = x^4\Psi^8/r^4$ the metric diverges as in leading order

$$g|_{x_C} \simeq \left(\frac{x_C}{r_{C_{lim}}}\right)^4 = \mathcal{O}\left(\tau_{zgp}^{4/3}\right) \tag{67}$$

and

$$g|_{x^+_{CEH}} \simeq \left(\frac{x^+_{CEH}}{r_{EH}}\right)^4 = \mathcal{O}\left(\tau_{zgp}^{4/3}\right) \tag{68}$$

are found.

Extending the study of [6], it turns out that also the gradient of g at the left-hand event horizon freezes, whereas making use of (27) and (28) the derivatives

$$\left.\frac{dg}{dx}\right|_{x_C} \simeq \frac{4x_C^3}{r^4_{C_{lim}}} = \mathcal{O}\left(\tau_{zgp}\right) \tag{69}$$

and

$$\left.\frac{dg}{dx}\right|_{x^+_{CEH}} \simeq -\frac{4C_{lim} x^{+\,6}_{CEH}}{r^9_{EH}} = \mathcal{O}\left(\tau^2_{zgp}\right) \tag{70}$$

at the throat and the right-hand event horizon are obtained.

Comparing these "zgp" late time statements with the corresponding ones obtained for even boundary conditions in Subsec. III A, i.e. comparing Fig. 2 with Fig. 1, one can see that in leading order identical slice sucking and wrapping is present at the right-hand event horizon and to its right. In the puncture evolution, however, almost no slice stretching occurs to the left of the throat since the "zgp" lapse collapses exponentially in time there. For this reason numerical evolutions of black hole puncture data imposing the "zgp" boundary condition are able to last significantly longer than runs forcing even boundary conditions.

Second example:
A one-parameter family of boundary conditions

Finally, a one-parameter family of boundary conditions ranging from odd to even and characterized by a constant multiplicator function in the linear combination (56), $\Phi = \text{const} \in [0,1]$, has been studied numerically in the context of isotropic grid coordinates. Here the lapse is determined by its time-independent value at the puncture given by

$$\alpha(\tau, x = 0) = 2\Phi - 1 \in [-1, 1] \quad \forall \tau. \tag{71}$$

The elliptic equation (55) for the lapse has been implemented in the regularized spherically symmetric code described in [24]. Using a shooting method and starting at the puncture with the value (71), to be interpolated there as the origin is staggered in between grid points, the derivative of the lapse has been determined such that when integrating outward a Robin boundary condition [25] is satisfied. All simulations shown in the following have been carried out using $30,000$ grid points for a resolution of $\triangle x = 0.001M$ to place the outer boundary at $x = 30M$.

It is worth mentioning that for negative values of the lapse no difficulties have been encountered numerically. In particular, evolving for odd boundary conditions up to $\tau_{odd} = 25M$, the deviations of lapse and metric components from their initial profiles have been found to be less than 0.1 per cent.

For the even lapse, however, note that the isometry condition (48) has not been enforced actively. In addition one should then remember that at late times the left-hand event horizon according to (51) gets arbitrarily close to the puncture, whereas the even lapse approaches the value $C_{lim}/r_{EH}^2 = 3\sqrt{3}/16 \approx 0.3248$ at x^-_{CEH} and is one at $x = 0$ as mentioned previously. Due to the rapidly steepening gradient close to the puncture the shooting method for the even lapse failed shortly after $\tau_{even} = 25M$.

In Fig. 3 on a logarithmic scale the decay of δ with time at infinity is shown for runs with constant values $\Phi = \{0, 1/8, 1/4, 1/2, 1\}$ and for the puncture evolution where $\Phi_{zgp} \to 1/2$ holds in the limit of late times. In this limit analytically an exponential decay on the timescale Ω/Φ is predicted, the corresponding slopes are shown in addition in this figure. Furthermore, in Fig. 4 for the same runs the slice stretching integrals $\mathcal{S}_H$ and $\mathcal{S}_G$, (58) and (59), are plotted together with the expected late time divergence being proportional to time at infinity. As one can see from these plots, the numerical results are in excellent agreement with analytical predictions. In particular, note that for "zgp" boundary conditions as compared to the run with $\Phi = 1/2$ more slice stretching arises initially. This happens since the puncture lapse starts with unit lapse everywhere whereas a "pre-collapsed" lapse profile is found when using the average of odd and even lapse from the beginning. At late times, however, identical slice stretching behavior is found as the two curves become parallel in both Fig. 3 and 4.

IV. CONCLUSION AND OUTLOOK

Slice stretching effects have been described which show up when maximally slicing the extended Schwarzschild spacetime while using a vanishing shift. Excluding odd boundary conditions where the static Schwarzschild metric is obtained and no slice stretching occurs, slice sucking and wrapping have been shown to arise at the throat of the maximal slices. In terms of δ in leading order in the limit $\delta \to 0$ the overall slice stretching has been characterized by integrals such as $\mathcal{S}_H$ and $\mathcal{S}_G$.

For even boundary conditions and two particular coordinate choices, namely logarithmic and isotropic grid coordinates, slice sucking and wrapping at the event horizon have been worked out explicitly.

Searching for favorable boundary conditions, it turned out that slice stretching effects described in terms of δ can show up arbitrarily late in terms of τ in numerical simulations if the corresponding lapse approaches the odd lapse and hence becomes negative in the left-hand part of the spacetime.

For numerically favorable boundary conditions demanding in addition the lapse to be non-negative, the latest possible occurrence of slice stretching has been found to take place for a lapse being at late times given by the average of odd and even lapse. The puncture lapse of [5] is precisely of this form and the puncture evolution of a Schwarzschild black hole is hence taking place in a numerically favorable manner.

Promising strategies for more accurate and longer lasting simulations make use of a shift (which reacts by pulling out grid points from the inner region as the slice stretching develops) and/or singularity excision (to cut away the troublesome part of the spacetime, an idea attributed to W. Unruh in [26], see e.g. [27]). For the shift several geometrically motivated conditions on the 3-metric (like minimal distortion [10], distance, area and expansion freezing [3] or Gamma-freezing [28]) have been proposed and studied numerically. To what extent it is possible to avoid slice stretching by making use of a non-trivial shift will be studied analytically for the maximally sliced Schwarzschild spacetime in a further paper [16].

Furthermore, as slice stretching by an intuitive argument is often attributed to the singularity avoiding behavior of the slicing, for the Schwarzschild spacetime the maximal slices will be compared in [29] to geodesic slices. The latter arise for evolutions with unit lapse and vanishing shift and correspond to freely falling observers which hit the Schwarzschild singularity within finite time.

Acknowledgments

It is a pleasure for me to thank M. Alcubierre, B. Brügmann, J.A. González and D. Pollney.

[1] S. L. Shapiro and S. A. Teukolsky, in *Dynamical Spacetimes and Numerical Relativity*, edited by J. M. Centrella (Cambridge University Press, Cambridge, England, 1986), p. 74 to 100.

[2] P. Anninos, K. Camarda, J. Massó, E. Seidel, W.-M. Suen, and J. Towns, Phys. Rev. D **52**, 2059 to 2082 (1995), gr-qc/9503025.

[3] P. Anninos, G. Daues, J. Massó, E. Seidel, and W.-M. Suen, Phys. Rev. D **51**, 5562 to 5578 (1995), gr-qc/9412069.

[4] For this reason terms like "grid stretching", "grid sucking" and "grid wrapping" appearing in some references are misleading and will not be used here.

[5] B. Reimann and B. Brügmann, Phys. Rev. D **69**, 044006 (2004), gr-qc/0307036.

[6] B. Reimann and B. Brügmann (2004), gr-qc/0401098, accepted for publication by Phys. Rev. D.

[7] B. Reimann, Master's thesis, Universität Potsdam, Germany (2003).

[8] J. York, in *Sources of Gravitational Radiation*, edited by

L. Smarr (Cambridge University Press, Cambridge, England, 1979).
[9] F. Estabrook, H. Wahlquist, S. Christensen, B. DeWitt, L. Smarr, and E. Tsiang, Phys. Rev. D **7**, 2814 to 2817 (1973).
[10] D. Bernstein, D. Hobill, and L. Smarr, in *Frontiers in Numerical Relativity*, edited by C. Evans, L. Finn, and D. Hobill (Cambridge University Press, Cambridge, England, 1989), p. 57 to 73.
[11] L. Brewin, Class. Quant. Grav. **19**, 429 to 455 (2002), gr-qc/0107030.
[12] D. Bernstein, D. Hobill, E. Seidel, L. Smarr, and J. Towns, Phys. Rev. D **50**, 5000 to 5024 (1994).
[13] R. Beig and N. O. Murchadha, Phys. Rev. D **57**, 4728 to 4737 (1998), gr-qc/9706046.
[14] B. Reinhart, J. Math. Phys. **14**, 719 (1973).
[15] M. Duncan, Phys. Rev. D **31**, 1267 to 1272 (1985).
[16] M. Alcubierre, B. Brügmann, D. Pollney, B. Reimann, M. Rumpfkeil, and E. Seidel (2004), in preparation.
[17] A. Einstein and N. Rosen, Phys. Rev **48**, 73 to 77 (1935).
[18] S. Brandt and E. Seidel, Phys. Rev. D **52**, 856 to 869 (1995), gr-qc/9412072.
[19] M. Koppitz, Ph.D. thesis, Universität Potsdam, Germany (2004).
[20] A. Gentle, D. Holz, A. Kheyfets, P. Laguna, W. Miller, and D. Shoemaker, Phys. Rev. D **63**, 064024 (2001), 0005113.
[21] M. Choptuik, Ph.D. thesis, University of British Columbia, Vancouver, Canada (1986).
[22] D. Eardley and L. Smarr, Phys. Rev. D **19**, 2239 to 2259 (1979).
[23] Here in order to avoid misunderstandings the spatial coordinates obtained during the evolution are refered to as "grid coordinates" to distinguish them from the initially implemented "coordinates". Note e.g. that unless odd boundary conditions are used neither (38) nor (46) hold at later times.
[24] M. Alcubierre and J.A. González (2004), gr-qc/0401113.
[25] J. York and T. Piran, in *Spacetime and Geometry: The Alfred Schild Lectures*, edited by R. Matzner and L. Shepley (University of Texas Press, Austin (Texas), 1982).
[26] J. Thornburg, Class. Quant. Grav. **4**, 1119 to 1131 (1987).
[27] E. Seidel and W.-M. Suen, Phys. Rev. Lett. **69**, 1845 (1992).
[28] M. Alcubierre, B. Brügmann, P. Diener, M. Koppitz, D. Pollney, E. Seidel, and R. Takahashi, Phys. Rev. D **67**, 084023 (2003), gr-qc/0206072.
[29] B. Reimann (2004), in preparation.

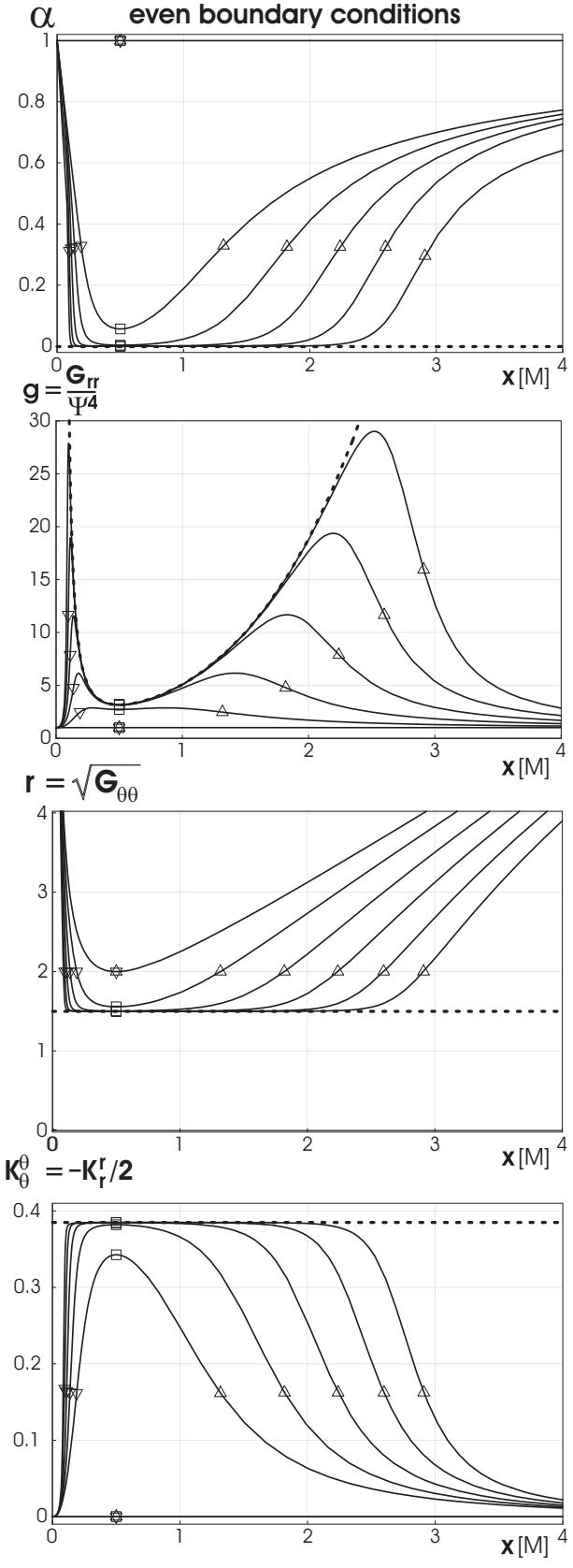

FIG. 1: The lapse function and components of both metric and extrinsic curvature are shown as obtained numerically at times $\tau_{even} = \{0, 5M, 10M, 15M, 20M, 25M\}$ for isotropic grid coordinates and even boundary conditions. The location of the throat and the left- or right-hand event horizon is denoted by boxes and down- or upward pointing triangles, respectively. In addition as dotted lines limiting curves are shown which hold in the limit $\tau_{even} \to \infty$ near the throat.

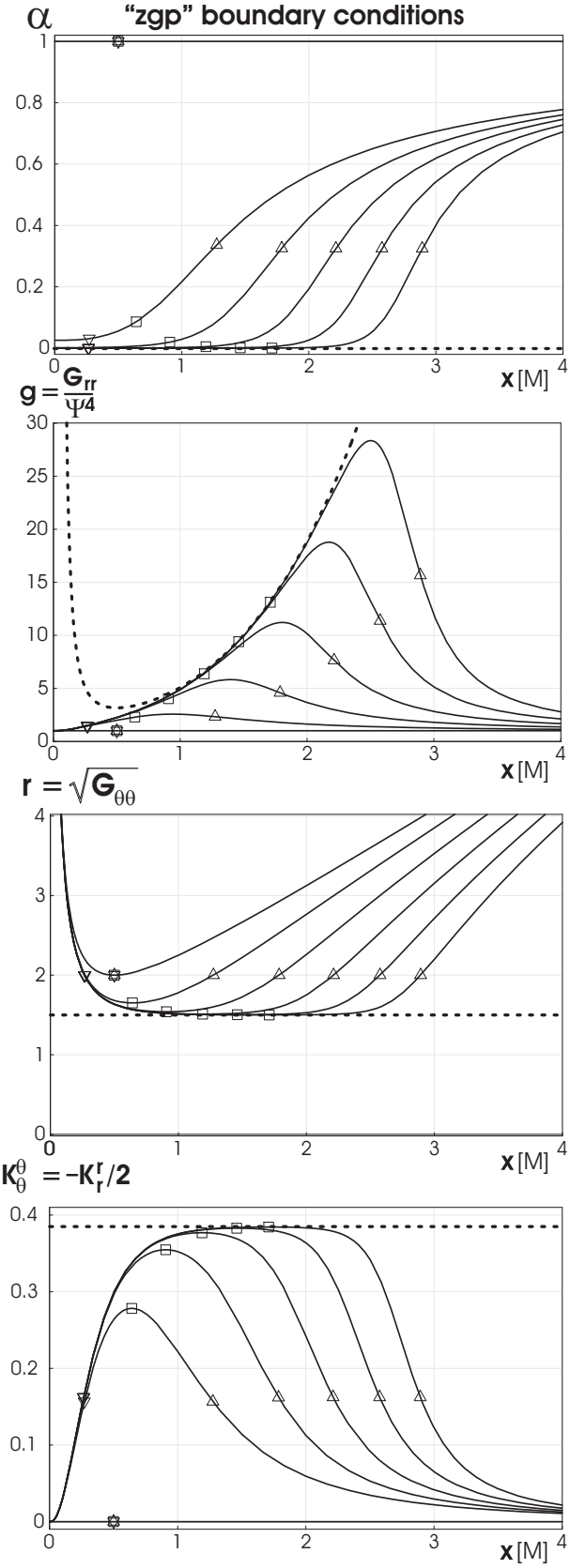

FIG. 2: For the puncture evolution corresponding to isotropic grid coordinates and "zgp" boundary conditions the geometric quantities as of Fig. 1 are shown in time steps of $\triangle\tau_{zgp} = 5M$. For $\tau_{zgp} \to \infty$ in a region near the throat the puncture lapse collapses to zero, the rescaled radial metric component can be described by $x^4\Psi^8/r^4_{C_{lim}}$, the Schwarzschild radius approaches the value $r_{C_{lim}} = 3M/2$ and the angular extrinsic curvature component has the limit $C_{lim}/r^3_{C_{lim}} = 2\sqrt{3}/9M \approx 0.3849/M$.

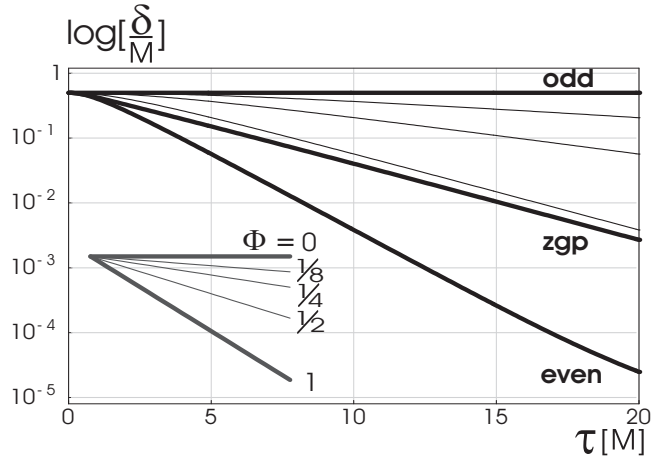

FIG. 3: The numerically observed difference in between the Schwarzschild radius at the throat r_C and its limiting value $r_{C_{lim}} = 3M/2$ is plotted on a logarithmic scale as a function of time. Here the thick lines correspond to odd ($\Phi = 0$), "zgp" ($\Phi_{zgp} \to 1/2$ in the limit of late times) and even ($\Phi = 1$) boundary conditions. The three thin lines from top to bottom are characterized by a constant multiplicator function having the value $1/8, 1/4$ and $1/2$. In the lower left corner the analytically predicted late time slopes are shown.

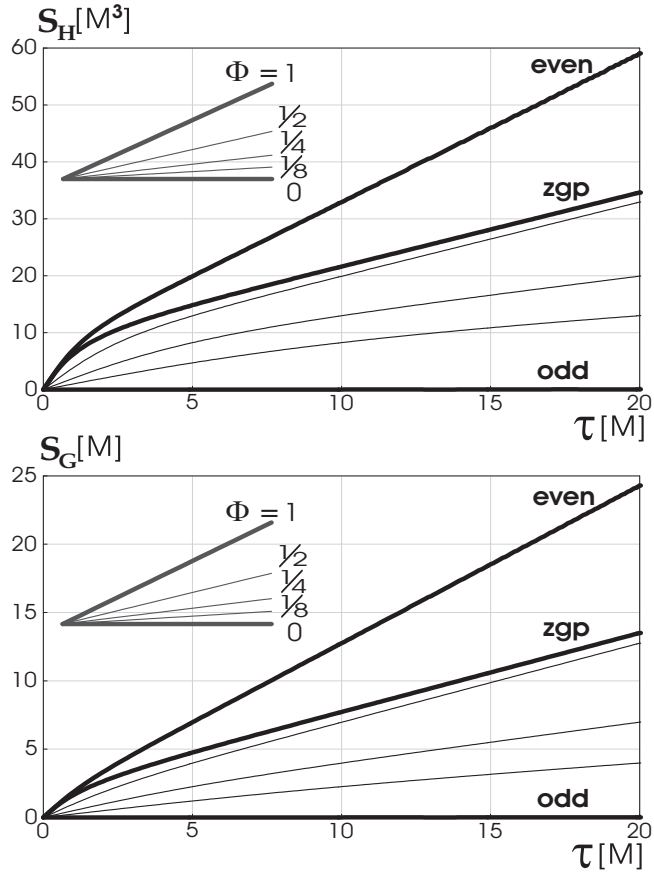

FIG. 4: The integrals $\mathcal{S}_H$ and $\mathcal{S}_G$ characterizing the overall slice stretching are shown for the puncture evolution and five members of the one-parameter family of boundary conditions having constant Φ, see text for details.